Prepared for submission to JINST

22[TH] iWoRiD
June 27, 2021 to July 1, 2021
online

Pixel chamber: a solid-state active-target for 3D imaging of charm and beauty

A. Mulliri,[a,1] M. Arba,[b] P. Bhattacharya, [a,2] E. Casula,[a] C. Cicalò,[b] A. De Falco,[a] M. Mager,[c] D. Marras,[b] A. Masoni,[b] L. Musa,[c] S. Siddhanta,[b] M. Tuveri,[b] G. Usai[a]

[a]*Dipartimento di Fisica, Università di Cagliari - Cagliari, Italy*
[b]*INFN, Sezione di Cagliari - Cagliari, Italy*
[c]*CERN*

E-mail: alice.mulliri@ca.infn.it

Abstract: The aim of the Pixel Chamber project is to develop the first "solid-state bubble chamber" for high precision measurement of charm and beauty.

In this paper we will describe the idea for the first silicon active target conceived as an ultra-high granular stack of hundreds of very thin monolithic active pixel sensors (MAPS), which provides continuous, high-resolution 3D tracking of all of the particles produced in proton-silicon interactions occurring inside the detector volume, including open charm and beauty.

We will also discuss the high-precision tracking and vertexing performances, showing that the vertex resolution can be up to one order of magnitude better than state-of-the-art detectors like the LHCb one.

Keywords: Detector modelling and simulations I, Particle tracking detectors

[1]Corresponding author.
[2]Now at Department of Physics, Adamas University - Adamas Knowledge City, Barasat-Barrackpore Road, Kolkata, 700126, India.

Contents

1 Introduction

Modern vertex detectors are based on cylindrical or planar layers of silicon sensors, generally immersed in a magnetic field. These detectors are used for precision measurements of the particles produced in the interactions and, in particular, of the dacay products of those with a long mean life, such as open charm and beauty.

Since in this kind of detectors vertices are calculated by extrapolating tracks reconstructed from hits in the tracking layers, it is important to have a very good spatial resolution and to be very close to the interaction point. However, the distance between the interaction point and the trackers poses an ultimate limitation in the achievable resolution of the vertex position.

In this regard, bubble chambers were very efficient active detectors with a good spatial resolution (O(10 μm)). E.g., strange particles were observed for the first time with a bubble chamber [**?**](figure **??**, left). Nevertheless, these trackers had a low time resolution (O(ms)) which is not suitable for experiments with a much larger event rate, such as modern experiments with higher event rates to study rare processes like charm and beauty production.

A silicon-based active-target capable to image open charm and open beauty particles in 3D, similar to a bubble chamber, does not exist. First ideas for such detectors were put forward almost 40 years ago [**?**], but the required technology became available only very recently.

This paper will describe the concept to build the first bubble chamber-like (figure **??**, right) high-granularity active-target based on silicon pixel sensors, called Pixel Chamber [**? ?**], capable to perform continuous, high-resolution (O(μm)) 3D tracking. Pixel Chamber is conceived to be a stack of hundreds of very thin monolithic active pixel sensors (MAPS).

We will then focus on the capabilities of the sensor in terms of tracks and vertex reconstruction.

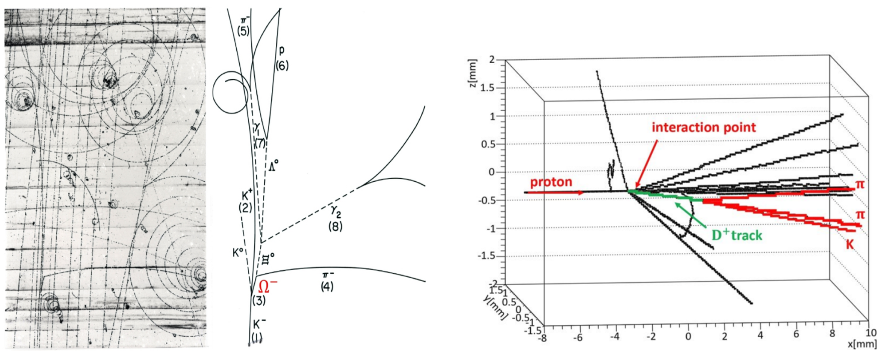

Figure 1. Left: image of the Ω discover with a bubble chamber [**?**]. Right: Geant4 simulation of p-Si interaction with the production of a D^+ meson inside Pixel Chamber.

2 Pixel Chamber

The most commonly used technology in the last 20 years in modern particle physics experiments is that of standard hybrid sensors. These sensors are characterized by an excellent time resolution and radiation hardness [? ?], and the silicon sensor is bump-bonded on the readout chip with a total thickness of few hundreds of μm.

A monolithic pixel cell contains a charge collection zone deposited on a silicon substrate in a commercial CMOS technology: the front-end electronics is integrated in the pixel cell reducing considerably the thickness of the sensor (O(50 μm)) and the production cost. Moreover monolithic sensors have a very good spatial resolution (around few μm).

For Pixel Chamber we propose to use the high-performance ALPIDE sensors developed for the last upgrade of ALICE vertex detector [?].

This sensor chip is produced in the TowerJazz 180 nm CMOS imaging process and contains a matrix of 1024 x 512 pixels [? ?] (pixel size ~ 29 x 27μm^2), with a thickness of 50 μm. The pixel contains a deep p-well which prevents PMOS transistors from collecting charge. This allows complex in-pixel amplification, shaping, discrimination and buffering to be implemented within the pixel. The sensor is designed to work at 50 kHz interaction rate with Pb beams and several hundreds kHz interaction rate with proton beams (LHC running conditions). It features a moderate radiation hardness, at the level of fluences of $10^{13} n_{eq}/cm^2$ and very low power consumption (~ 40 mW/cm^2).

The basic unit of Pixel Chamber is a stack of 9 ALPIDE sensors called A9 stack shown in figure **??**, left.

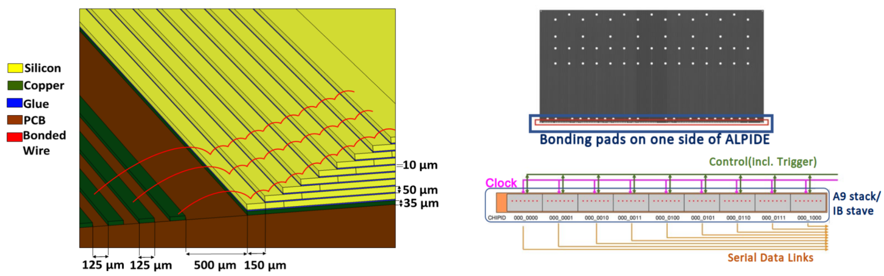

Figure 2. Left: the A9 stack scheme showing the wire bonding of the staggered sensors on a PCB. Right-top: bonding pads on ALPIDE. Right-bottom: clock, control and data signals from the A9 stack (the same as the ALICE ITS Inner Barrel stave [? ?]).

The nine sensors are arranged in a staggered fashion with an offset of 150 μm to provide the space for wire bonding of the sensor pads. The pads that provide access to the signal and power circuits of the sensor, reside on one side of the surface of the sensor along its length (figure **??**, right-top). Between two sensors there will be a thin layer of 10 μm thick of electrically insulating glue. The total thickness of the A9 stack is 530 μm. The 9 ALPIDE sensors in the A9 stack have individual 1.2 Gbps serial data lines, a shared bi-directional differential control and monitoring line and a shared differential clock line (figure **??**, right-bottom). The data, control, monitoring and clock signals are interfaced on a PCB through wire bonds.

Pixel Chamber is a set of 24 A9 stacks for a total of 216 sensors that form the complete stack (thickness: 13 mm) along the scheme shown in figure **??**, left. Considering the sensors offset, the active chamber volume is 30x13x10 mm^3.

In Pixel Chamber, signal and power lines will be distributed by a combination of rigid and flex PCBs. The rigid part will host the wire bonds and will extend 1.2 mm inwards from the periphery of the first sensor of the A9 stack (figure **??**, right). The flex PCBs is a continuation of the rigid PCBs and will be connected to a patch-panel interfaced to the Readout Units, as shown in figure **??**, right.

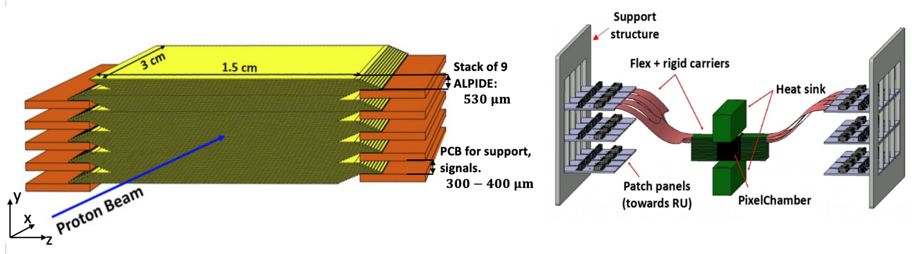

Figure 3. Left: view of the Pixel Chamber stack. Right: Pixel Chamber integrated with flexible and rigid PCBs connected to patch-panels for interfacing with the readout system of ALICE ITS.

The detector performance was studied with Geant4 (G4) [**?**]. The geometry has been implemented to simulate a stack of 216 ALPIDE sensors. The reference system is shown in figure **??**, left: the x-axis defines the beam direction (figure **??**, right), while the y-axis is directed vertically along the stack.

A beam of 400 GeV protons is sent towards the detector (figure **??**, left, figure **??**, right) to obtain inelastic proton-Si interactions inside the sensor. Since G4 does not provide for the production of charm particles in inelastic interactions, charm production has been simulated considering, for instance, D^0 or $D^{\pm}$ mesons. Charm particles are produced in the interaction point (primary vertex) according to kinematics parameters (rapidity and transverse momentum) evaluated with POWHEG[**?**].

From the G4 simulation, a dataset is obtained for particles produced in p-Si interactions, including charm decay products. The dataset contains various information including the coordinates of the center of the pixels crossed by a particle (hits) and useful information for the Monte Carlo (MC) truth, such as momentum, energy, PDG code and production vertex of the particles that generate a hit in the detector.

3 Track reconstruction algorithm

A track reconstruction algorithm based on hits density has been developed and tested with G4 simulations.

The first step of the tracking algorithm is the search of hit pixel neighbours. Pixel coordinates are defined in terms of integer indices i, j, k along the x, y, z axes and a hit pixel is defined as a neighbour of a given pixel if the discrete distance (in terms of indices) between them is 1 (figure **??**). This operation can require a long computational time so, to optimize it, hits are first ordered by increasing the i index using the quicksorting algorithm [**?**].

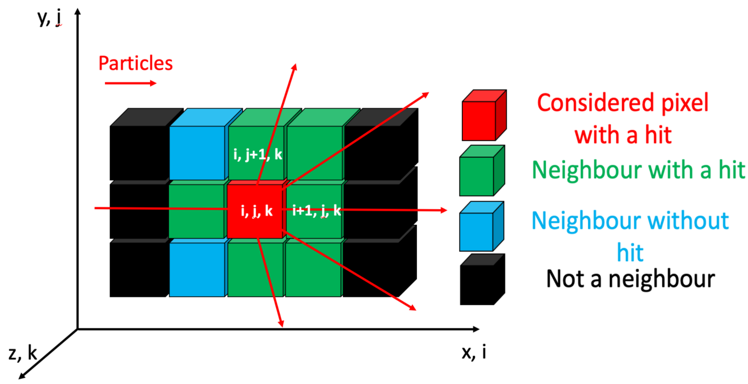

Figure 4. Illustration of pixels neighbours with index coordinates.

This density-based grouping is qualitatively similar to DBSCAN [**?**]. However, to avoid that tracks that originate from a common point (vertex) are merged to a single cluster, it is necessary to apply an upper limit on the number of neighbors (N_{neigh}). A hit is added to a cluster if $1 < N_{neigh} < 4$ (figure **??**), otherwise it is considered as a noise point.

At this point most of the tracks are split in small clusters which are then fit with a linear track model. The coordinate errors in the fit are the expected standard deviation for a position measurement with a digital pixel of a given pitch. The parameters vector obtained from the fit contains the y, z coordinates of a reference point along the line and the y, z direction cosines normalized to the x-direction cosine (α, β). These parameters are used to find compatible clusters that should belong to the same track and should therefore be merged.

Two clusters are considered compatible and can be merged if they have compatible direction cosines, their extreme points are closer than 70 μm and the reduced χ^2 (χ^2/ndf) of the merge resulting track is smaller than 1.5. With this first merge, many short clusters are merged to form longer tracks.

At this stage, many noise points can still be present. For this reason, clustering algorithm on noise points is repeated with less stringent conditions on N_{neigh} (i.e., $1 < N_{neigh} < 5, 1 < N_{neigh} < 7$).

The merge procedure is then repeated until no clusters can be merged any more. The last step of the reconstruction is to try to merge the residual noise points to the reconstructed tracks. A noise point can be merged to a track if their distance is smaller than 40 μm and if the χ^2/ndf of the resulting track is smaller than 2.5.

At the end of the reconstruction, most of the rectilinear, hadronic tracks are well reconstructed, while non-rectilinear tracks are still split (figure **??**, left). Non-rectilinear tracks are mostly due to low energy particles, such as δ electrons, and therefore of little interest. Some hadronic tracks collinear with the beam proton are still broken too. The reason is that at very forward rapidity the hit density is very high because tracks are very close to each other and therefore it is difficult to perform a good reconstruction.

The track reconstruction efficiency is calculated using MC truth informations as the ratio of the MC hadronic tracks that produce more than 50 hits and the number of reconstructed tracks compatible with them. In this case tracks are compatible if they have compatible direction cosines and the the smallest distance between their extreme points is less than 70 μm. The track reconstruction efficiency is almost 80% (figure **??**, right). However, if the interaction occurs close to the end of the detector, hadronic tracks are short and difficult to resolve. For this reason we consider a cut to exclude events where the interaction point is in the last 10 mm (V_x < 5mm) of the detector. The track reconstruction efficiency rises to more than 90%.

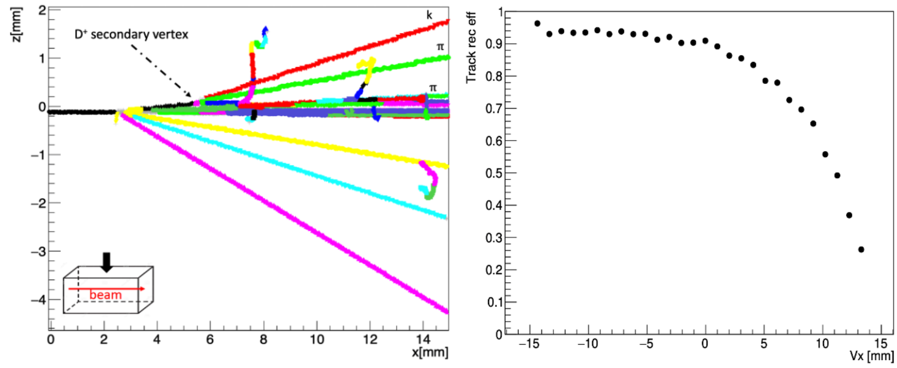

Figure 5. Left: display of the reconstructed tracks of one event with a proton-silicon inelastic interaction and D^+ decay products tracks. Right: average track reconstruction efficiency, as a function of the interaction point;

4 Vertex reconstruction

4.1 Interaction point (primary vertex)

The algorithm for vertex reconstruction is based on a method used in several other experiments, such as LHCb [**?**] and ALICE and earlier, CERES [**?**] and NA60.

The aim is to determine the x_v, y_v, z_v vertex coordinates, while the tracks are not refitted.

We define h_i the vector of the y_v, z_v coordinates.

The initial values of x_v, y_v, z_v (vertex seed) are set as the coordinates of the last point of proton track which is reasonably close to the interaction point. The proton track is identified as the one that begins at the entrance to the detector.

For each reconstructed track with more than 50 points (n_{pts} > 50) and χ^2/ndf < 2.5, the vector q_i of y, z coordinates corresponding to x_v is calculated based on the fitted parameters.

$$q_i = \begin{pmatrix} y_{0i} - (x_v - x_{0i})\alpha_i \\ z_{0i} - (x_v - x_{0i})\beta_i \end{pmatrix} \tag{4.1}$$

Using h_i, q_i, the impact parameter χ^2_{IP} is evaluated:

$$\chi^2_{IPi} = (q_i - h_i)^T V_i^{-1} (q_i - h_i) \tag{4.2}$$

where V_i is the track covariance matrix obtained from the track fit.

A weight W_T is assigned to each track on the basis of its χ^2_{IP}. The weight depends on the ratio between the χ^2_{IP} and the so called Tukey constants C_T and is set to 0 if $\chi^2_{\mathrm{IP}} > C_T$.

This allows to avoid to associate to the primary vertex tracks than could worsen the vertex estimation.

The primary vertex χ^2_{PV} is obtained summing each track χ^2_{IP} weighted by $\mathrm{W_T}$, and it is then minimized to obtain the vertex coordinates:

$$\chi^2_{PV} = \sum_{i=1}^{n_{tracks}} \chi^2_{IPi} W_{Ti} \tag{4.3}$$

The procedure is iterative and the χ^2_{PV} is recalculated at each iteration for decreasing values of $\mathrm{C_T}$. The initial value of $\mathrm{C_T}$ is set to 10^6 to avoid convergence in a local minimum. At each iteration, the vector $\mathrm{h_i}$ is updated and the values of χ^2_{IP} and $\mathrm{W_T}$ are recalculated. In this way, the tracks that in a specific iteration had a weight equal to zero are retested and if their weight is different from zero they contribute to the fit. The iteration is stopped when χ^2_{PV} has converged to a stable value.

Figure **??** shows the distribution of the $\chi^2_{\mathrm{PV}}/\mathrm{ndf}$. There is a peak at zero due to primary vertices with only one or two tracks. If the track multiplicity is 1 the interaction occurs at the end of the detector and no track except the proton verifies the conditions necessary to be associated with the vertex.

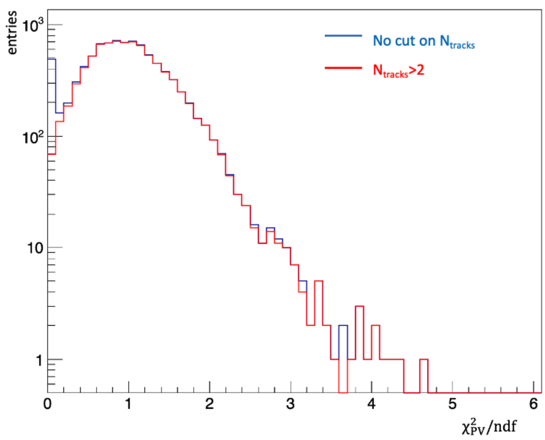

Figure 6. $\chi^2_{\mathrm{PV}}/\mathrm{ndf}$ PV distribution. Blue: total distribution. Red: distribution requiring that the multiplicity of tracks associated to the primary vertex is bigger than 2.

If we consider reconstructed vertices with $\chi^2_{\mathrm{PV}}/\mathrm{ndf} < 2.5$ and track multiplicity bigger than 2, the efficiency of the vertex reconstruction is 93%. Removing interactions occurred in the last 10 mm ($\mathrm{V_x} < 5$mm) of the detector, the reconstruction efficiency reaches 97%.

The resolutions on the vertex coordinates are obtained as the standard deviation of the residuals calculated as the difference between the fitted vertex coordinates and the coordinates from the MC truth. Resolutions are shown in fig **??**, top as a function of the primary vertex track multiplicity ($\mathrm{n_{tr}}$). They improve significantly for increasing $\mathrm{n_{tr}}$. E.g. for $\mathrm{n_{tr}} > 2$, $\sigma_x \sim 16\mu$m and increases up to 5μm for $\mathrm{n_{tr}} > 25$.

In figure **??** the vertex coordinates resolutions versus track multiplicity are shown and compared to LHCb [**?**]. Although the two experiments have very different setups and different beam energies, it is interesting to observe that with Pixel Chamber it is possible to obtain resolutions that are about one order of magnitude better than those obtained with LHCb.

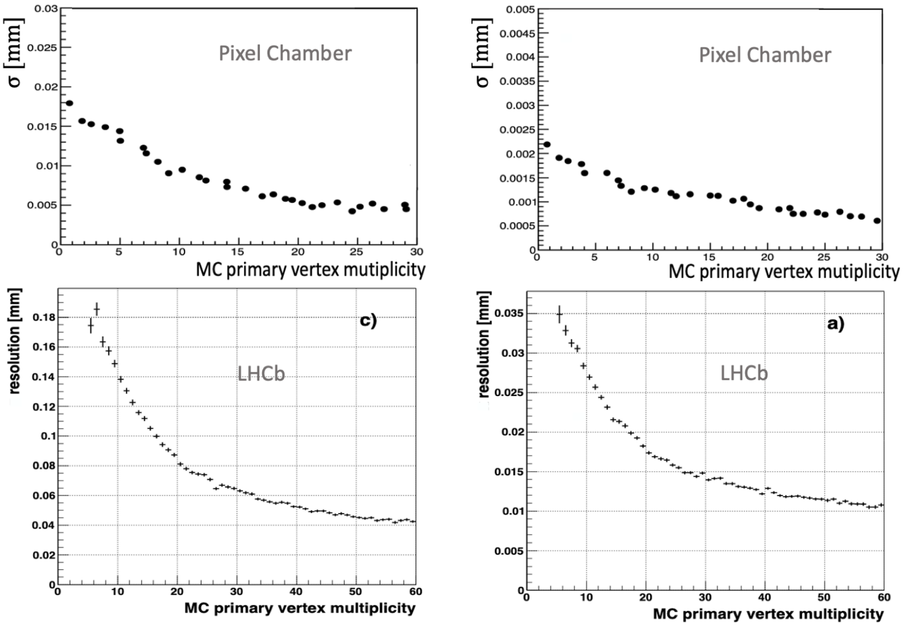

Figure 7. Primary vertex resolutions as a function of the number of tracks associated to the primary vertex reconstructed in Pixel Chamber (top) and LHCb (bottom) [**?**] left panels show resolutions along the beam axes, right panels show resolutions along a transverse axis.

4.2 D^0 decay vertex

The algorithm used for the reconstruction of primary vertices has also been used to reconstruct D^0 decay vertices, although with appropriate modifications. First the vertex fit is performed on pairs of tracks (with $n_{pts} > 50$ and $\chi^2/ndr < 2.5$) as the D^0 meson decays in two charged particles. The fit is performed on all combinations of pairs of tracks not associated to the primary vertex. Secondly the vertex seed is the closest point to the primary vertex of one of the two tracks under test.

The secondary vertex reconstruction is performed on all the events with a primary vertex with $\chi^2/ndr < 2.5$, $n_{tr} > 3$ and $V_x < 5mm$. Many secondary vertices can be found in each event and the D^0 vertex candidate is selected as the closest to the reconstructed primary vertex.

Using MC truth informations, it is possible to obtain the efficiency of the D^0 vertex reconstruction which is $\sim$ 80%.

There are many reasons for the presence of 20% of misidentified vertices: the secondary vertex is very close to the interaction point and one or both tracks are incorrectly associated with the primary vertex; it can happen that one or both tracks are broken and do not fit the requirements to be used in the vertex fit.

The residuals distributions obtained as the difference between the MC and reconstructed vertex coordinates are shown in figure **??**. The resolutions on the secondary vertices coordinates are the standard deviations of the residuals distributions (figure **??**) and are 25 μm along the beam axis, 5 and 4 μm along the two transversal axes. These resolutions show that the potentialities of reconstruction of the secondary vertices of the D^0 are excellent even if it is necessary to improve further the algorithm.

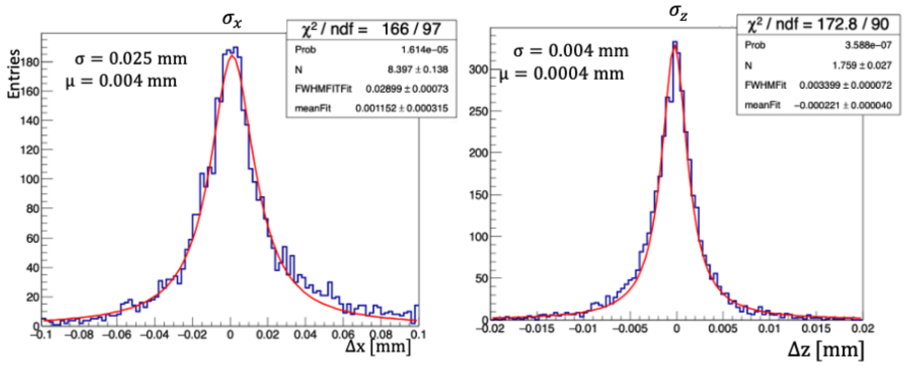

Figure 8. Residuals distributions for secondary vertices obtained as the difference between the MC and reconstructed vertex coordinates.

5 Conclusions and outlook

In this paper we described briefly the idea of Pixel Chamber, a three dimensions (3D) active target pixel matrix. Simulations studies performed with Geant4 show that it is possible to obtain a high efficiency for the reconstruction of hadronic tracks and the primary and secondary vertex inside the detector. The position of the vertices can be measured with very high precision.

Track reconstruction could be further improved taking into account multiple scattering. This will be done adding a Kalman filter fit to the algorithm. In addition, machine learning and neural networks might also be used to improve tracks and vertices reconstructions.

We are currently exploring the possibility of adding a silicon telescope for momentum measurements after Pixel Chamber. Momentum measurements together with the high precision with which it is possible to determine the position of the vertices inside the sensor could allow to obtain excellent results in the study of charm and beauty particles.

References

[1] Barnes V. E. et al., *Observation of a Hyperon with strangeness minus three*, *Phys. Rev. Lett.,* **12** (1964) 204

[2] Bellini G. et al., *Miniaturization of High-Energy Physics Detectors (Springer),* (1983)41-55

[3] Usai G. et al., *Pixel Chamber: A universal silicon heavy-flavor imager for fixed-target measurements of charm and beauty with unprecedented precision,* Project funded by the Sardinian Regional Government

[4] Mulliri A. et al., *Pixel chamber: A solid-state bubble chamber for imaging of charm and beauty, NCC,* **44 C** (2021) 6

[5] Allison J, et al., *Geant4 Developments and Applications*, *IEEE Transactions on Nuclear Science,* **53** (2006) 279-278

[6] Perrin-Terrin M., *The NA62 GigaTracker*, *Proceedings of the 24th International Workshop on Vertex Detectors (Vertex 2015),* **154** (2015) 16

[7] Apollinari G. et al., *High-luminosity large hadron collider (HL-LHC)*, **1** *CERN Yellow Reports: Monograph* (2017) 1-516

[8] Aglieri Rinella Gianluca on behalf of the ALICE Collaboration, *The ALPIDE pixel sensor chip for the upgrade of the ALICE Inner Tracking System)*, **245** *Nucl. Instrum. Methods A,* (2017) 853

[9] ALICE collaboration, *Upgrade of the ALICE Experiment: Letter Of Intent*, *J. Phys.* **41** (2014)087001

[10] ALICE collaboration, *The ALPIDE pixel sensor chip for the upgrade of the ALICE Inner Tracking System*, *J. Phys.* **41** (2014)087002

[11] J. Schambach et. al., *A Radiation-Tolerant Readout System for the ALICE Inner Tracking System Upgrade*, *IEEE Xplore,* (2018) 1-6

[12] Alioli S. et. al., *A general framework for implementing NLO calculations in shower Monte Carlo programs: the POWHEG BOX*, **06** *JHEP,* (2010)

[13] JaJa J., *A Perspective on Quicksort*, **2** *Comput. Sci. Eng.,* (2000)43

[14] Ester M. et al., *A Density-Based Algorithm for Discovering Clusters in Large Spatial Databases with Noise*, *Proceedings the Second International Conference on KDD, AAAI Press* (1996)226-231

[15] Kucharczyk M., Morawski P. and Witek M., *Primary Vertex Reconstruction at LHCb*, *LHCb-PUB* (2014)44

[16] Agakichiev G. et al., *A new robust fitting algorithm for vertex reconstruction in the CERES experiment*, **394***Nucl. Instrum. Methods* (1997)225